Experimental and theoretical evidence for oriented aggregate crystal growth of CoO in a polyol

Thomas Gaudisson, Surender K Sharma, Rahamane Mohamed, B. Sitamtze Youmbi, Nicolas F Menguy, Florent Calvayrac, Mahamadou Seydou, Souad Ammar-Merah

CrystEngComm

DOI: 10.1039/d0ce01525c

Experimental and Numerical evidence of an oriented aggregate crystal growth of CoO in polyol

Thomas Gaudisson,[a] Surender K. Sharma,[a] Rahmane Mohamad,[a] B. Sitamtze Youmbi,[b] Nicolas Menguy,[c] Florent Calvayrac,[b,*] Mahamadou Seydou,[a,*] and Souad Ammar-Merah[a,*]

Monodispersed about 5 nm sized CoO crystals were prepared by forced hydrolysis of cobalt(II) acetate in diethyleneglycol (DEG) solvent. The adsorption of the solvent molecules on these primary nanocrystals caused their in-situ oriented aggregation resulting in the precipitation of textured submicrometer-sized polycrystals. X-ray diffraction, Infrared spectroscopy, Transmission Electron Microscopy and Thermogravimetry analyses coupled to *ab-initio* modeling were applied to understand the adsorption mechanism of the alcohol moieties and the role of the molecule-to-surface and molecule-to-molecule interactions in the crystal growth mechanism of these polycrystals. We showed that DEG moieties are mainly adsorbed at the top of the cobalt (100) surface atoms and the process does not involve the whole molecule but only one of its extreme oxygen atoms. As a consequence, adsorbed DEG molecules exhibit an extended configuration which is favorable to intermolecule hydrogen bonding from one covered nanocrystal to another. Interestingly, at high surface coverage, the energy required for DEG attachment to the crystal surface is found to be 18.6 kJ/mol per molecule, while that required for hydrogen bonding between a bearing molecule and a neighbor one is found to be 36,4 kJ/mol per molecule, meaning that the collective departure of an assembly of DEG from the surface of CoO nanocrystals is therodynamically easier, leading thus to the observed final morphology.

Introduction

Transition metal oxides form an important class of functional materials. They are widely used in various technological fields: catalysis, battery-based energy storage, electrochromism, ferroelectricity and microelectronic among others. The reduction of their particle size down to some nanometers, the control of their size distribution and the adjustability of their aggregation state can greatly affect their properties and then their applicative potential. Several methods were already used in order to produce size and shape controlled oxides nanoparticles (NPs) but among all of them colloidal chemistry appeared as the most versatile and the most efficient for the desired goal. Colloidal chemistry usually proceeds through two growth mechanism, diffusion and aggregation. In water, without any dispersant agent in the reaction medium, the initially formed primary nanocrystals exhibit hydroxyls groups at their surface, which lead to their aggregation and the formation of polycrystals, water acting as a binder [1]. In non-aqueous reaction medium, the aggregation kinetics is slower due to less surface hydroxyl groups and to greater solvent viscosity. So even if aggregation can not be avoided, these operating conditions give the nanocrystals enough cushion to rotate finding potentially the low-energy configuration interface and forming thus oriented aggregates [2], a kind of pseudo-single crystals. In presence of dispersing agent, the aggregation process can be avoided leading to single crystals by diffusion growth. In fact, the control of the final morphology is achieved by finely tuning the crystal surface energy via preferential adsorption of the additives onto specific crystallographic facets [3-6]. Usually such a morphological control permits producing anisotropic in shape NPs [7] but it can also reduce the particle size by quenching the growth of the formed crystal nuclei [8-11], leading to the formation of small isotropic single crystals instead of large polycrystals. In some favourable cases, the primary nanocrystals achieve crystallographic alignment despite spatial separation from one another leading to mesocrystals, which can fuse into oriented aggregates, leading to epitaxied clustered nanocrystals also called pseudo-single crystals [12]. The transition from mesocrystals to pseudo-single crystals attracts a lot of attention because it is a promising method for creating advanced artificial materials with distinct micro- and nanostructures. Indeed, very often the resulting pseudo-single crystals exhibit physical properties, such as magnetic ones, corresponding to larger crystals, still different from those of their bulk counterpart as from those of their constituting primary nanocrystals [13-14]. It must be pointed out that this transition is not completely understood. It is not yet clear how the organic species initially adsorbed on the primary nanocrystals depart from the surfaces. Do they desorb or do they decompose during the oriented aggregation process?

In this context, we aim to combine experimental and theoretical evidence of oriented aggregation growth of transition metal oxide particles, namely cobalt monoxide CoO, in diethyleneglycol (*DEG*) using a well-known soft chemistry method, the so-called polyol-mediated synthesis. This method consists of a forced hydrolysis of

metallic salts in a polyol solvent, the molecules of which may be in-situ adsorbed and desorbed, leading to a controlled crystal growth of the desired oxide particles. They typically act as dispersing and growth orienting agents.

Results and discussion

A Experimental evidence of the pseudo-single crystal behaviour

The XRD pattern of the recovered light brown powder exhibits almost broadened peaks matching very well with the rock-salt like structure of the cobalt oxide phase. The refined cell parameter was found to be a = 4.267(5) Å, very close to that of bulk CoO (ICDD n°00-042-1300). Besides, MAUD analysis allowed concluding that the produced powder is constituted by almost strain free and quite isotropic in shape nanocrystals of about 15(1) nm in size (Table 1)

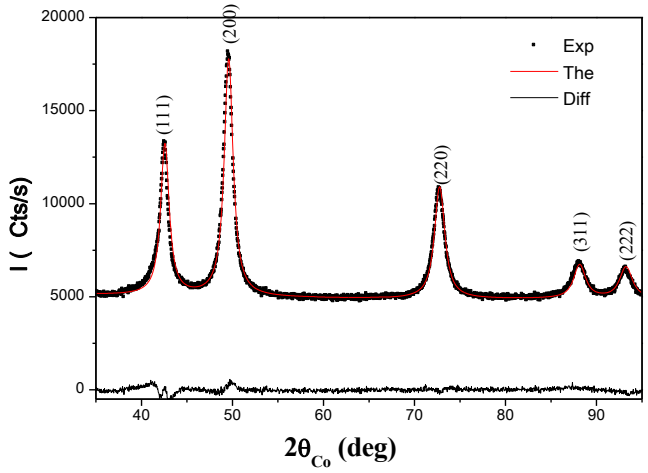

Figure 1. The recorded (scatters) and calculated (continuous line) XRD patterns of the produced oxide powder. The residual curve is given at the bottom of the figure to illustrate the fit quality (Bragg reliability factor R_B = 1.4).

Table 1. The average CoO crystal size, crystal micro-deformation, primary particle size and aggregate diameter, as inferred from XRD and TEM analyses, respectively.

$<L_{XRD}>$ / nm	$<\varepsilon>$ / %	$<d_{TEM}>$ / nm	$<D_{TEM}>$ / nm
15 ± 1	0.13	5 ± 1	100 ± 20

Transmission Electron Microscopy (TEM) observations show that these nanocrystals are aggregated forming almost spherical sub-micrometer sized polycrystalline particles (Figure 2). From the recorded high resolution (HRTEM) micrographs a textured cluster structure appears. Clearly, the identified polycrystals are in fact formed by about 5 nm single crystals exhibiting common crystallographic plane orientations. This epitaxy is suggested by the collected Laüe-type Fourier Transform (FFT) pattern on one representative polycrystal border, matching very well with the cubic CoO structure and it is confirmed by the electron diffraction recorded on one isolated submicrometer-sized polycrystals.

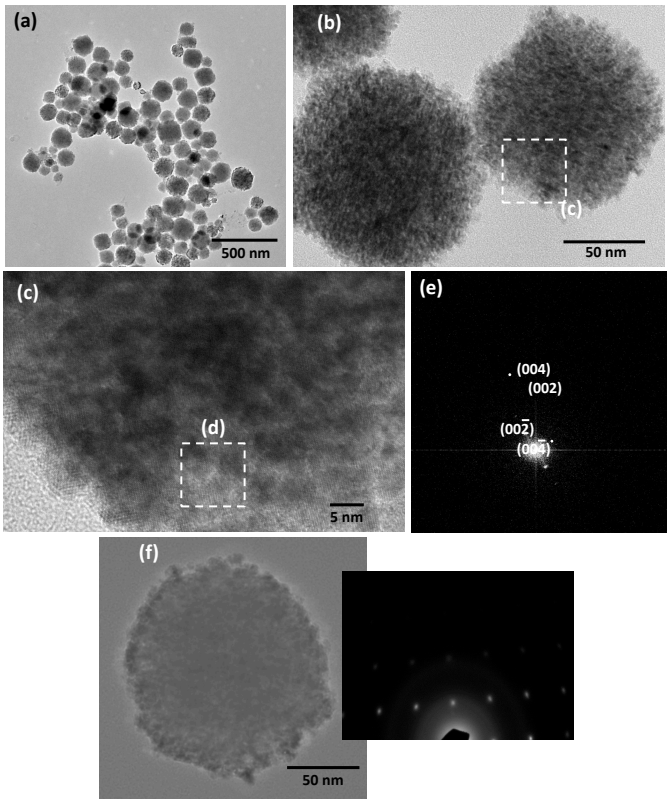

Figure 2. TEM micrographs recorded on (a) an assembly of CoO particles, (b) a couple of representative particles. A zoom is given on (c) selected area and the FFT pattern of the selected (d) area is calculated (e) and fully indexed within the rock-slat CoO structure. Electron diffraction pattern of one CoO polycrystal is also given (f) to highlight its Laue-type.

Once again a typical Laüe pattern was obtained, meaning that the prepared CoO particles are in fact pseudo-single crystals (Figure 2f), explaining the observed discrepancy between the average crystallite size inferred from XRD (15 nm) and that inferred from TEM (5 nm). Indeed, XRD allowed measuring an average coherent domain length, labelled here $<L_{XRD}>$, which may differ from the exact crystal size. Hence, in the case of epitaxial nanocrystals, one may *a priori* assume that the determined $<L_{XRD}>$ exceeds the real size of primary NPs, giving in our case coherence lengths of about 15 nm instead of the measured 5 nm by TEM. Such a feature has already been observed in the case of polyol-made textured nanocrystalline transition metal oxide aggregates [13-15].

These observations suggest that CoO crystal growth in polyol is a two-step process. At the beginning, CoO crystals nucleate and start growing by diffusion, leading to primary particles with an average diameter of 5 nm. The surface of these primary particles interact with the polyol solvent molecules, through the complexing ability of the later [16], which form a kind of steric barrier toward cobalt solute diffusion. In these conditions, a diffusion mechanism becomes less easy to achieve. So, for an optimized arrangement of the polyol adsorbates on the surface of the CoO nanocrystals, intermolecular interactions proceed, leading to the organisation of these nanocrystals into large clusters. The transition from this cluster microstructure to a polycrystal one is then favorited thanks to a collective departure of the adsorbates from the interstitial spaces.

So, a series of experiments were thus conducted to confirm this mechanism. First, FTIR spectroscopy was performed on the as-produced powder. Interestingly, the recorded spectrum presents the signature of organic residue (Figure 3), meaning that the produced particles are still organically contaminated.

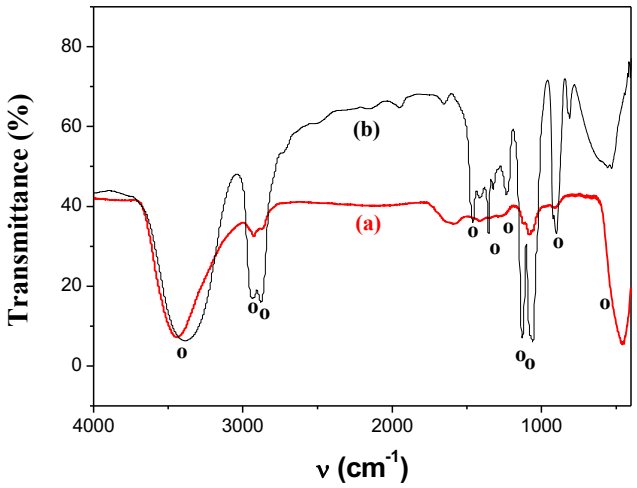

Figure 3. FTIR spectrum of polyol-made CoO powder (a) compared to that of free DEG (b). The main characteristic vibration bands of DEG are annotated by "o"

Typically, *DEG* specie was clearly identified. Its presence is characterized by the stretching ν(O-H), ν(C-H) and ν(C-O) vibration bands at 3382, 2931-2971 and 1125-1075 cm^{-1}, respectively [17,18].

An attentive spectrum lecture does not allow us to completely exclude the presence of acetate as organic residue in the recovered CoO powder. Indeed, this molecule is usually characterized by the stretching symmetric and asymmetric ν(COO) vibration bands at around 1600 and 1400 cm^{-1} [19-21]. These bands are not clearly observed but a small bump can be pointed out at about 1506 and 1424 cm^{-1} in the recorded particle spectrum. So, even though these bumps may mark the presence of acetate, the relative peak intensities of these peaks compared to those of *DEG* allows us to neglect their presence. This hypothesis is supported by the fact that acetates are introduced in the reaction medium as precursors in a finite quantity while *DEG* molecules are used as solvents in a large excess. So, even both, acetate and *DEG*, are good Co^{2+} ligands and both are able to adsorb on the CoO crystal surface, the amount of adsorbed acetate is statistically significantly smaller than that of adsorbed *DEG*. On other words, *DEG* is expected to the most representative particle's adsorbate.

To tentatively quantify the adsorbed moieties on the produced CoO particles, TG analysis was performed with a special emphasis on their weight losses, which should proceed at temperatures close to the boiling points of each potentially present molecules, water ($E°_{water}$ = 100°C), acetate/acetic acid ($E°_{acetic\ acid}$ = 118°C) and/or *DEG* ($E^0_{diethyleneglycol}$ = 245°C) and/or at temperatures close to the thermal decomposition point of these species ($T^0_{acetate}$ > 355°C [22] and $T^0_{diethyleneglycol}$ = 250-255°C [23]). Indeed, adsorbates may depart from an inorganic surface by boiling or by decomposition depending on the strength of its attachment to the surface.

The recorded thermogram clearly evidence two main exothermic features, a narrow weight loss at around 200-240°C and a broadened mass increase from 240 to 600°C. The former corresponds to *DEG* molecule departure, while the latter coincides with CoO oxidation into Co_3O_4 (the formation of Co_3O_4 was confirmed by XRD analysis of the TG residue). The temperature of DEG departure is closer to DEG boiling point than to its decomposition point, meaning that these solvent molecules are not so strongly attached to the polyol-made CoO particles.

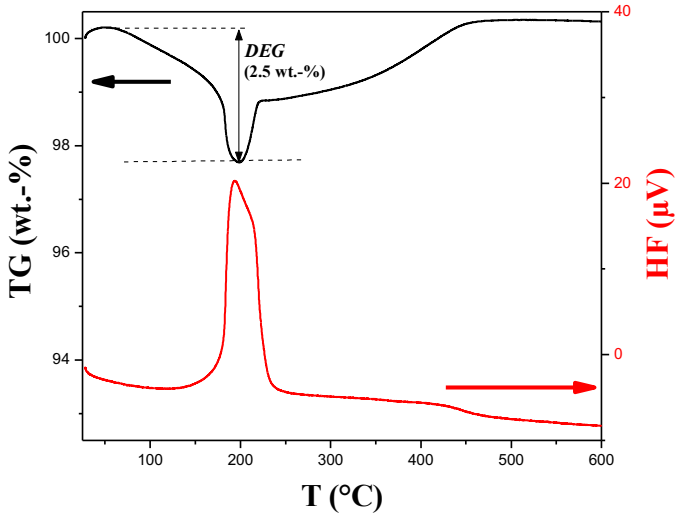

Figure 4. Temperature dependence of the relative mass loss (TG) and the heat flow (HF) of the as-produced CoO particles during heating in air. The horizontal dashed lines delimit the main weight loss, which proceed around DEG boiling point.

Moreover, the measured weight loss allows determining the DEG weight content in the produced particles. It is found to be very low about 2 wt.-%, in agreement with the location of this organic matter only in outer CoO particle layer. Indeed, by a simple geometrical model it is possible to estimate the *DEG* weight content on the produced particles within the hypothesis of *DEG* adsorption as a dense monolayer at the surface of the sub-micrometer sized secondary particles. Taking into account the surface of one sub-micrometer-sized particle ($S_{particle} = 4\pi R_{particle}^2$) and the binding area of one *DEG* ligand on the particle surface ($A_{DEG} = a_{DEG}^2$, where a_{DEG} is the side length of the quadratic binding area of one ligand), the amount of surface bound ligands can be calculated by dividing the former with the latter. So, assuming each CoO particle as a sphere of a radius equal to the average TEM particle radius ($R_{particle}$ = 50 nm) and fixing the a_{DEG} to 0.7 nm, which is a reasonable value compared to those proposed by Binder et al. for various 1,2-diols [24,25] as it is consistent with the computed distance between two adjacent *DEG* molecules on the CoO surface (see modelling section), and using the molecular weight of the surface bound ligand (M_{DEG} = 108 $g.mol^{-1}$) it is possible to determine the theoretical mass fraction of the surface bound ligands with respect to the total mass of the particle. The total particle mass is assumed to be equal to the product of bulk CoO volumic mass (ρ_{CoO} = 6.44 $g.cm^{-3}$) by the average particle volume ($V_{particle} = \frac{4}{3}R_{particle}^3$):

$$DEG\ (\text{wt.-\%}) = 100\,\frac{\frac{M_{DEG}}{N_A}\frac{S^2_{particle}}{A_{DEG}}}{(\rho_{CoO}V_{particle})+\left(\frac{M_{DEG}}{N_A}\frac{S^2_{particle}}{A_{DEG}}\right)} \qquad \text{Eq. 1}$$

$$DEG\ (\text{wt.-\%}) = 100\ \frac{\frac{M_{DEG}}{N_A \times a_{DEG}^2}}{\left(\frac{\rho_{CoO} R_{particle}}{3} + \frac{M_{DEG}}{N_A \times a_{DEG}^2}\right)} \qquad \text{Eq. 2}$$

These equations give a value of 1.03 wt.-%, in good agreement with the experimental value inferred from TG analysis (2.5 wt.-%).

B Modelling *DEG* interaction on CoO surface

To model *DEG* molecule grafting on the surface of CoO particles, the molecule was first relaxed. Figure 4 displays the optimized geometry.

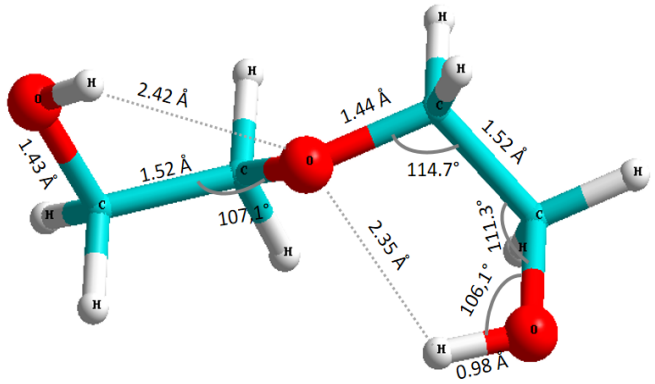

Figure 4. Optimized *DEG* molecule geometry, with its interatomic distances and selected angles displayed.

As usual, finding a global minimum for adsorption is challenging. Therefore, only the most probable geometries from physical considerations have been considered as starting configurations. We focused our attention on the mechanism involving oxygen atom from free diethyleneglycol and cobalt cation from nude CoO crystal surface. First, we studied the adsorption of isolated molecule on this surface and the absorption of an assembly of them. Weaker hydrogen bond interactions may proceed, but they are often neglected. They typically connect a proton from a terminal *DEG* hydroxyl group with an oxygen surface anion. In fact, the most probable interaction between *DEG* and CoO surface is driven by the complexing properties of the polyol, through which its oxygen atoms interact with cobalt surface cations. Within the Green classification [26], the resulting complexing reactions may involve only one oxygen atom of a L unidente ligand or a X_2 bridging ligand, or two or three oxygen atoms of a L_2 or L_3 chelating or bridging ligand. These configurations depend on the degree of saturation of the coordination sphere of surface cobalt cations, which itself depends on the crystallographic face type. Previous calculations have shown that cobalt oxide crystals exhibit preferentially (100) crystallographic faces [27]. In the CoO (001) surface, they are only fivefold coordinated $[CoO_5]^{8-}$ complexes corresponding to edge truncated octahedra. An adsorbate bound to that surface will probably fill the vacancy of the missing oxygen ion in the direction normal to the surface to strengthen the ligand field [28] in other to achieve the six fold coordinated configuration. Only one oxygen atom of a L type ligand may be engaged within such a geometry. A single oxygen atom a X_2 ligand bridging two cobalt cations as well as a pair of oxygen atoms of a L_2 ligand attached to a same cobalt cation can not respect such a Co-O bonding directionality. So, different adsorption sites were thus investigated for *DEG* oxygen atoms, tacking in mind that *DEG* ligands would preferentially interact on the CoO surface as L unidentate ligands. So, to be as exhaustive as possible, different *DEG* adsorption geometries, including the bridging ones, were thus simulated, fully relaxing each system, and estimating the adsorption energy per molecule, ΔE_{ads}. This energy was computed as the difference between the grafted molecule on the surface, $E_{Surface+DEG}$, and the energy of isolated molecule, E_{DEG}, and that of bare surface $E_{Surface}$:

$$\Delta E_{ads} = E_{Surface+DEG} - (E_{Surface} + E_{DEG}) \qquad \text{Eq.3}$$

The geometries with the lowest adsorption energies and the shortest oxygen to surface bound distances are assumed to be representative of the most stable ones (Table 2). A simple comparison between the calculated energies shows that a vertical attachment on a single Co cation as unidentate ligand (TOP_Co) is the most stable while a parallel attachment on pair of Co cations as bridging ligand (PRL) is the less stable (-141.5 versus -12 kJ/mol). These two extremal geometries are illustrated in Figure 5. The energies calculated for other geometries, like those called BRIDGE (X_2 ligand) and TOP_O (hydrogen bond plus probably charge transfer), are also given for information (Table 2).

Adsorption site	ΔE_{ads}(kJ/mol)	$d_{O...Surface}$ (Å)
BRIDGE	-23,6	2.48
TOP_ O	-78,5	2.32
TOP_Co:	-141,5	2.28
PRL	-12,0	2.46

Table 2. Adsorption energies and distances for the adsorption sites. The $d_{O...Surface}$ distance is the vertical spacing between the cobalt oxide surface and the oxygen atom of isolated *DEG* molecule.

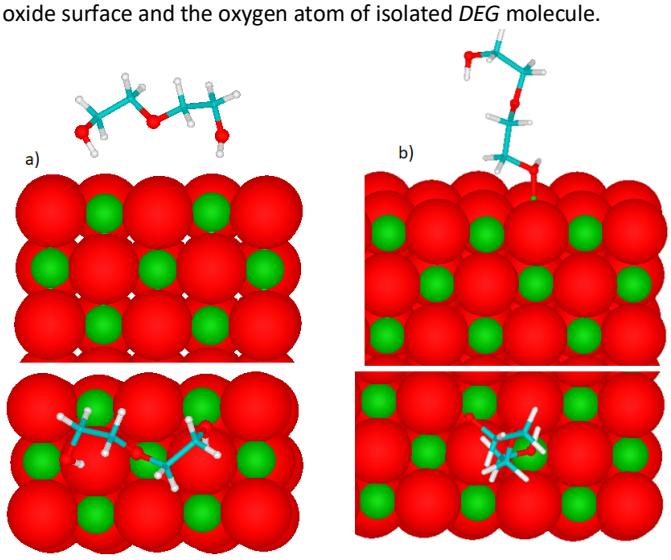

Figure 5. Side and top views of the adsorption sites of *DEG* on CoO (001) surface: (a) PRL and (b) TOP. Green balls are cobalt atoms, red balls are oxygen, cyan balls are carbons and white balls are hydrogens.

These calculations confirm our expectations. The adsorption does not involve the whole molecule, but only the oxygen atom situated at one of its extremities. Within this configuration, the adsorption distance is 2.28 Å. It is slightly larger than the Co-O distance in bulk

CoO crystal (2.11 Å), but quite close, compared to the adsorption energies calculated for the other geometries (Table 2).

To the best of our knowledge, very few works are reported on CoO (001) surface structure and electronic properties [27]. Most of the literature on rock-salt oxide deals with the NiO system. But, even if NiO exhibits similar properties than CoO, the (001) surfaces of this compound exhibit topological differences, as experimentally evidenced by scanning tunneling microscope (STM) experiments [29]. There is nevertheless a unique experimental observation performed by Felton et al. on CoO surface relaxation [30], which reported that surface atoms in CoO relax by less than 3% with respect to bulk spacing.

According to Sitamtze-Youmbi et al. calculations, CoO (001) plans exhibit a small rumpling and at their topmost surface layer, the relaxation height of Cobalt ions is different from that of Oxygen ions [27]. The surface relaxation of O ions is of almost 2.3% with respect to the bulk lattice interlayer spacing of 2.13 Å, contrary to the cobalt ions for which it is only 1.5%. However, both types of atoms exhibit almost the same relaxation in the inner atomic crystal layers, about 2.1% [27]. Whatever the case, relaxations are outward the calculated 2.28 Å distance, in agreement with Felton et al. observations [30].

Thanks to this geometrical arrangement, mutual interactions (mainly hydrogen bonds and van der Waals) between the adsorbed molecules on one seed and another may proceed, making the involved seeds attached to each other within a crystallographic order, leading to the formation of oriented nanoclusters. If the adsorbates may depart from the internal interfaces, these clusters may fuse leading to the formation of secondary pseudo-single crystals.

We know from TG analysis that *DEG* molecules are not so strongly linked to the particle surface. We know also from the relevant literature, that *DEG* molecules, as other polyols, are strongly polar and can establish strong hydrogen bonds allowing them to self-assemble [31].

For this raison, we built *DEG* one-dimensional chain and two-dimensional network (Figure 6) and we evaluated the stability of these theoretical architectures by calculating their cohesion energy. The cohesion energies per molecule of 1D and 2D networks were computed by the difference between the energies of the supra-molecular network (E_R) and the isolated molecules $N \times E_{DEG}$, where N is the number of molecules in the unit cell (a primitive cell contains 2 molecules):

$$\Delta E_{coh} = (E_R - N \times E_{DEG})/N \qquad \text{Eq. 4}$$

One way to tackle the *DEG* desorption process concerns the competition between the molecules self-interactions and their interactions with the surface. So, the assembly of molecules on CoO (001) was studied and the adsorption energy per molecule of the network were computed and compared to the results on isolated molecules in the previous section. The adsorption energy per molecule is computed as the difference between the energies of the optimized complex surface-network and the isolated network and bare surface relaxed separately as follows:

$$\Delta E_{ads} = (E_{Surface+R} - (E_{Surface} + E_R))/N \qquad \text{Eq. 5}$$

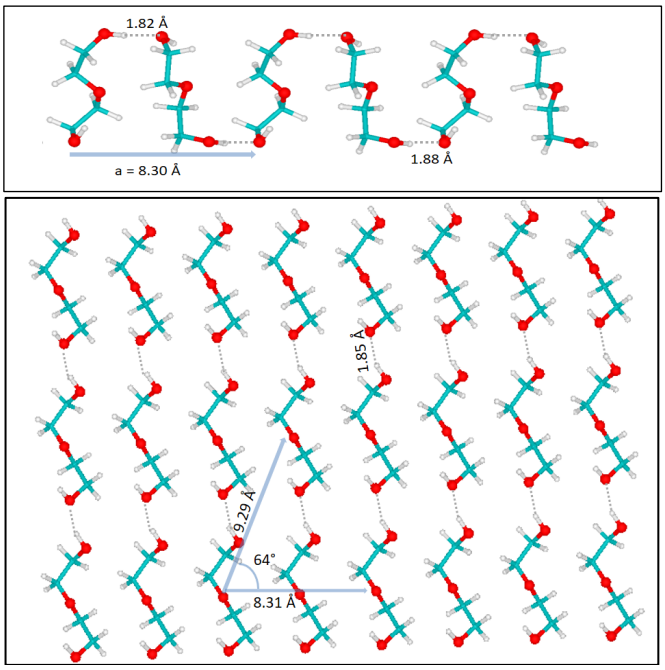

Figure 6. Self-assembly of *DEG* molecules: (a) representation of the primitive cell and (b) its 2D network.

The calculated cohesive energies per molecule are found to be -43.6 and -36.4 kJ/mol for 1D and 2D assemblies, respectively. The stability is assured by the hydrogen bonds and van der Waals interactions between polar and apolar backbones, respectively. The adsorption energies of networks are found lower than isolated molecules. The difference comes from the molecular self-interactions that disadvantage their adsorption on surface. Table 3 summarizes the adsorption energies of isolated and networks compared to the cohesion energies.

	Isolated *DEG*	1D DEG chain	2D DEG network
ΔE_{coh}(kJ/mol)	0	-43,6	-36,4
ΔE_{ads}(kJ/mol))	-141,5	-26,7	-18,6

Table 3. Comparison between adsorption energies per molecule of the isolated molecule and their 1D and 2D assemblies.

It appears clearly that the cohesion energy is significantly higher than the adsorption energy leading to the collective desorption of molecules from the surface as it can be seen in Figure 7. In fact, in this case, one out of two layers are desorbed in order to optimize the head-head hydrogen bonds between molecules.

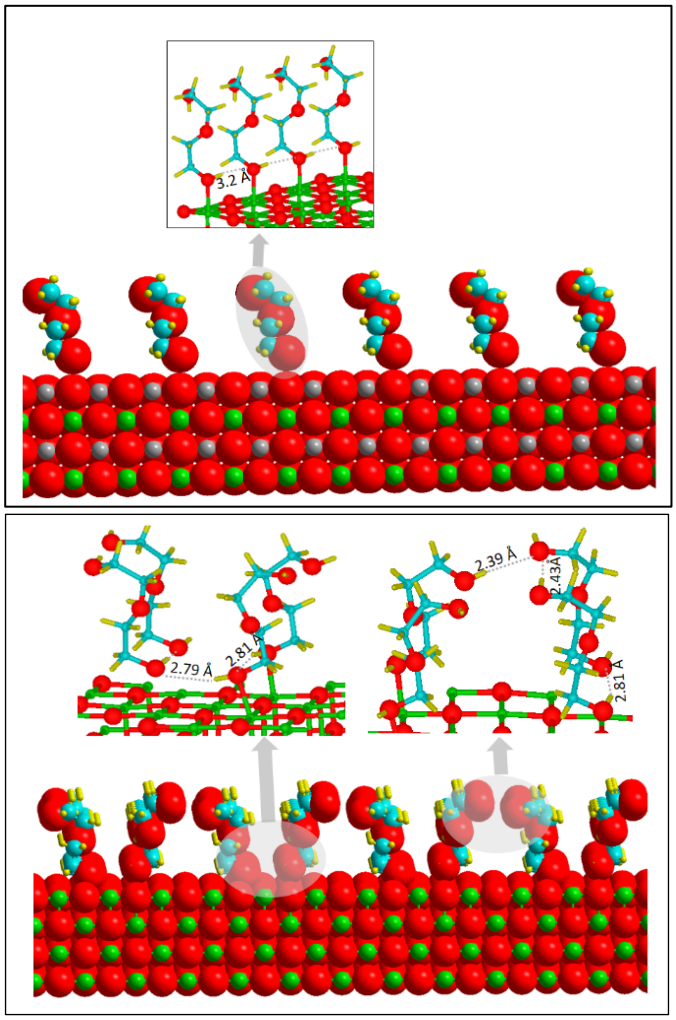

Figure 7. Representation of the adsorbed *DEG* molecules as a monolayer onto CoO (100) surface within (top) parallel and (bottom) inclined geometries.

It is clear now, from these numerical demonstrations and from our previous experimental clues, that the *in-situ* formed CoO/DEG mesocrystals merge into pseudo-single crystals thanks to the collective desorption of *DEG* molecules from the surface of the primary CoO nanocrystals. It must be pointed out that the role of *DEG* is crucial. Indeed, polyol-mediated CoO synthesis was already achieved using *DEG* as solvent while adding polyvinyl pyrolidone (*PVP*) polymer as dispersing agent. Within these operating conditions, CoO particles of almost the same size (around 80 nm in diameter) were obtained as polycrystals and not at all as pseudo-single crystals [32]. In all evidence the competition between *DEG* and *PVP* adsorption and desorption on the surface of primary CoO nanocrystals did not allow CoO/DEG mesocrystals formation highlighting the importance of the nature of adsorbates, their surface attachment configuration and the strength of their intremolecular interactions for the guidance of the in solution crystal growth mechanism toward an oriented aggregation one.

Materials and Methods

A Chemicals

Metal acetate salt $Co(CH_3COO)_2.4H_2O$ and diethyleneglycol solvent (*DEG*) were purchased from ACROS. All the products were used without any further purification

B Particle synthesis

CoO NPs were obtained by forced hydrolysis in polyol medium [33]. Typically, 3.11 g of $Co(CH_3COO)_2.4H_2O$ and 0.63 mL of distilled water were dissolved in 250 mL of *DEG* and heating up to 180°C for 18 hours under mechanical stirring. After that, the cooled suspension was centrifuged and washed several time with ethanol to obtain a clean powder which was subsequently dried in air without specific cautions

C Particle characterisation

The structure of NPs was analyzed using X-ray diffraction (XRD) using a Panalytical diffractometer equipped with a X'celerator detector and a Cobalt X-ray tube (λ = 1.7889 Å) in a θ-θ Bragg-Brentano reflexion configuration in the 10-100° angular range (with a step of 0.016°). Their microstructure was first checked by a Rietveld analysis of the recorded XRD pattern using MAUD (version 2.55) software [34], focusing on the determination of the average crystal size, $<L_{XRD}>$, the average micro-deformation, $<\varepsilon>$, induced by interne micro-strains. It when second checked by Transmission Electron Microscopy (TEM) observation using a JEOL-100-CX II microscope operating at 100 kV, with a special emphasis on the particle size and size distribution. Statistical counting of the particles from the obtained TEM micrographs was performed using SAISAM software (Microvision Instruments) and then calculating the surface-average particle diameter $<D_{TEM}>$ and its standard deviation σ, considering a spherical particle shape.

D Organic residue identification

Adsorption of organic residue was first investigated using FTIR spectroscopy using KBr technique. IR spectra were recorded on a FT-IR Perkin-Elmer 1750 spectrophotometer in the transmittance mode between 4000 and 500 cm^{-1} with a resolution of 4 cm^{-1} (at least 20 scans). Besides Thermal analysis was performed with a Thermo Gravimetry/Differential Thermal Analyzer (TG/DTA) Setaram TGA92 apparatus from room temperature up to 600°C (10°C/min) under a flow of air at 80 mL/min.

E DEG adsorption/desorption modeling

The attachment of diethyleneglycol derivatives, mainly *DEG* at the CoO particle surface, was modeled using an *ab-initio* approach. It was built in the framework of density functional theory. Calculations were performed with Vienna Ab-Initio Simulation Package (VASP 5.4.1) [35]. The electron-ion interactions were described by the projector augmented wave (PAW) method [36]. The convergence of the plane-wave expansion was obtained with a cut off of 500 eV. The sampling in the Brillouin zone was performed on a grid of k-points separated by 0.5 $Å^{-1}$ for the geometry optimizations. The functional of Perdew-Burke-Ernzerhof (PBE) was used under generalized gradient approximation (GGA) [37]. Dispersion effect is added using Grimme's DFT-D3 method [38]. The particles were considered as large enough that the site where a DEG molecule will bind is almost locally flat and then the system particle+*DEG* could be treated as a surface+*DEG* one, with periodic boundary conditions for the surface and a vacuum in the direction orthogonal to the surface. CoO (001) surface was modelled by a

slab of five layers containing 4 or 8 atoms per layer. The topmost layers were allowed to relax until all components the forces on atoms are less than 0.05 eV.Å^{-1}; and the two bottom layers fixed at their bulk positions. In order to achieve artificial periodicity, a vacuum of 25 Å was added in the direction perpendicular to the surface. This vacuum size was found enough to handle any artificial electric field due to periodic boundary conditions, and therefore no need to apply a dipole correction [39]. Similar approach was adopted to model CoO (110) and CoO (111) surfaces. Metal oxides possess strong electronic correlations that may be corrected to reproduce the correct band gap and magnetic moment. The Dudarev method [40] is used with Hubbard effective parameters found to U = 9 eV and J = 1 eV capable to reproduce the experimental band gap and magnetic moment of the bulk. These parameters are in line with previous studies [27,41].

Conclusions

The oriented aggregation crystal growth mechanism of sub-micrometer-sized CoO polycrystals, in a polyol reaction solution, was investigated coupling experimental evidence of the pseudo-single crystal behavior of the obtained particles, called here secondary particles, and polyol solvent molecules, adsorption and desorption modelling on and from the surface of nanometer-sized CoO seeds, called here primary particles. The role of polyol solvent molecules in the oriented aggregation of these seeds, issued from homogeneous nucleation and diffusion growth, was highlighted. The polyol is a diethyleneglycol, involving two terminal hydroxyl groups around an ether one. We demonstrated that this complexing molecule is preferentially adsorbed in a top geometry at the (001) CoO crystal faces, interacting one surface cobalt cation by only one of its terminal oxygen atoms. Through hydrogen bonding and van der Waals interactions between these adsorbed molecules on one seed and another lead to well-arranged clusters. But since these mutual molecular interactions are thermodynamically much more favourable than the ligand to surface complexing interactions, these molecules depart collectively from the seed surfaces giving to the formed cluster a pseudo-single crystal behaviour. As far as we know, this model is the only one able to explain and predict the evolution of the polyol-made CoO particle morphology.

Conflicts of interest

The authors declare that they have no financial interests or personal relationships that could influence the work reported here.

Acknowledgements

The French ANR (Agence Nationale de la Recherche) and CGI (Commissariat à l'Investissement d'Avenir) are acknowledged for their financial support through Labex SEAM grant (ANR-11-LBX-086, ANR-11-IDEX-0502). The authors want also to thank GENCI/IDRIS and CRIHAN national and regional facilities for computational time (projects x2010096171, x2011096171, x2012096171 and 007, respectively). Finally they want to thank Dr. John Lomas (Universite de Paris) for his helpful advices.

Notes and references

1 N. L. Wu, L. F. Wu, I. A. Rusakova, A. Hamed, A. P. Litvinchuk, *J. Am. Ceram. Soc.,* 1999, **82**, 67.
2 A. P. Alivisatos, *Science,* 2000, **289**, 736.
3 L. Bisson, C. Boissiere, L. Nicole, D.; Grosso, J.-P. Jolivet, C. Thomazeau, D. Uzio, G. Berhault, C. Sanchez, *Chem. Mater*., 2009, **21**, 2668.
4 T. He, D. Chen, X. Jiao, *Chem. Mater*., 2004, **16**, 737.
5 Y. Yin, P. Alivisatos, *Nature,* 2005, **437**, 664.
6 T. Thomson, M. F. Toney, S. Raoux, S. L. Lee, S. Sun, C. B. Murray, B. D. Terris, *J. Appl. Phys.,* 2004, **31**, 149.
7 Y. Soumare, C. Garcia, T. Maurer, G. Chaboussant, F. Ott, F. Fiévet, J.-Y. Piquemal, G. Viau, *Adv. Func. Mater*., 2009, **19**, 1971.
8 E. M. Wong, P. G. Hoertz, C. J. Liang, B.-M. Shi, G. J; Meyer, P. C. Searson, *Langmuir*, 2001, **17**, 8362.
9 N. S. Pesika, Z. Hu, K. J. Stebe, P. C. Searson, *J. Phys. Chem. B* 2002, **106**, 6985.
10 T. Hyeon, S. S. Lee, J. Park, Y. Chung, H. B. Na, *J. Am. Chem. Soc.* 2001, **123**, 12798.
11 S. Sun, H. Zeng, *J. Am. Chem. Soc.* 2002, **124**, 8204.
12 V. M. Yuwono, N. D. Burrows, J. A. Soltis, R. Lee Penn, J. Am. Chem. Soc. 2010, 132, 2163.
13 R. Valenzuela, S. Ammar, F. Herbst, R. Ortega-Zempoalteca, *Nanosci. Nanotechnol. Lett.*, 2011, **3**, 598.
14 T. Gaudisson, M. Artus, U. Acevedo, F. Herbst, S. Nowak, R. Valenzuela, S. Ammar, *J. Magn. Magn. Mater.* 2014, **370**, 87.
15 Z. Beji, M. Sun, L. S. Smiri, F. Herbst, C. Mangeney, S. Ammar, *RSC Adv.*, 2015, **5**, 65010.
16 F. Fievet, S. Ammar-Merah, R. Brayner, F. Chau, M. Giraud, F. Mammeri, J. Peron, J.-Y. Piquemal, L. Sicard, G. Viau, *Chem. Soc. Rev*., 2018, **47**, 5187.
17 A. Abdallah, T. Gaudisson, R. Sibille, S. Nowak, W. Cheikhrouhou-Koubaa, K. Shinoda, M. François, M. S. Ammar, *Dalton Trans*., 2015, 44, 16013.
18 D. Knetsch, W. L. Groeneveld, *Inorg. Chim. Acta.* 1973, **7**, 81.
19 L. Poul, N;Jouini, F. Fiévet, *Chem. Mater.,* 2000, **12**, 3123.
20 R.Boubekri, Z. Beji, K. Elkabous, G. Viau, S. Ammar, F. Fiévet, H. J. von Bardeleben, A. Mauger, *Chem. Mater.,* 2009, **21**, 843-855.
21 S. Ammar, A. Helfen, N. Jouini, F. Fievet, I. Rosenman, P. Monié, *J. Mater. Chem.,* 2001, **11**, 186.
22 L. S. Bell, D. A. Palmer, H. L. Barnes, S. E. Drummond, *Geochim. Cosmochim. Acta*, 1994, **58**, 4155.
23 H. Lecompte, J. J. Liggat, *Polym. Degrad. Stab.,* 2006, **91**, 681e689.
24 W. H. Binder, H. C. Weinstab, *Monatshefte Chem*., 2007, **138**, 315.

25 W. H. Binder, H. C. Weinstab, R. Sachsenhofer, *J. Nanomaterials*, 2008, 383020.
26 M. L. H. Green, *J. Organomet. Chem.,* **1995**, *500*, 127.
27 B. Sitamtze Youmbi, F. Calvayrac, *Surf. Sci.,* 2014, 621, 1.
28 H. Zheng, *Physica B,* 1995, **212**, 125.
29 M. R. Castell, S. L. Dudarev, G. A. D. Briggs, A. P. Sutton, *Phys. Rev. B,* 1999, **59**, 7342.
30 R. C. Felton, M. Prutton, S. P. Tear, M. R. Welton-Cook. *Surf. Sci*., 1979, **88**, 474.
31 Y. Chen, Y. Ozaki, M. A. Czarnecki, *Phys. Chem. Chem. Phys.,* 2013, **15**, 18694.
32 N. Izu, I. Matsubara, T. Uchida, T. Itoh, W. Shin, *J. Ceram. Soc. Jap.*, 2017, **125**, 701.
33 L. Poul, S. Ammar, N. Jouini, F. Fiévet, F. Villain, *Solid State Sci.,* 2001, **3**, 31.
34 L. Lutterotti, S. Matthies, H. R. Wenk, *IUCr: Newsletter of CPD* 1999, **21**, 14.
35 G. Kresse, J. Hafner, *Phys. Rev. B,* 1993, **47**, 558.
36 J. P. Perdew, K. Burke, M. Ernzerhof, *Phys. Rev. Lett.,* 1996, **77**, 3865.
37 H. J. Monkhorst, J. D. Pack, *Phys. Rev. B,* 1976, **13**, 5188.
38 S. Grimme, J. Antony, S. Ehrlich, H. J. Krieg, *Chem. Phys.,* 2010, **132**, 154104.
39 L. Bengtsson, *Phys. Rev. B,* 1999, **59**, 12301.
40 S. L. Dudarev, G. A. Botton, S. Y. Savrasov, C. J. Humphreys, A. P. Sutton, *Phys. Rev. B,* 1998, **57**, 1505.
41 U. D. Wdowik, K. Parlinski, *Phys. Rev. B,* 2007, **75**, 104306.